Analysis of low-lying states, neutron-core excitations, and electromagnetic transitions in tellurium isotopes $^{130-134}$Te

H. K. Wang,[1,2,3,*] S. K. Ghorui,[4] Z. Q. Chen,[5] and Z. H. Li[5,†]

[1]*College of Physics and Telecommunication Engineering, Zhoukou Normal University, Henan 466000, China*
[2]*School of Physics and Astronomy, Shanghai Jiao Tong University, Shanghai 200240, China*
[3]*GSI Helmholtzzentrum für Schwerionenforschung GmbH, 64291 Darmstadt, Germany*
[4]*Institute of Modern Physics, Chinese Academy of Sciences, Lanzhou 730000, China*
[5]*School of Physics and State Key Laboratory of Nuclear Physics and Technology, Peking University, Beijing 100871, China*

(Received 23 August 2020; accepted 26 October 2020; published 11 November 2020)

The neutron-rich $^{130-134}$Te isotopes are investigated by large-scale shell-model calculations with the extended pairing plus multipole-multipole force (EPQQM model). The orbits of $(0g_{7/2}, 1d_{5/2}, 1d_{3/2}, 2s_{1/2}, 0h_{11/2})$ are included for both proton and neutron model space, while two more neutron orbits $(1f_{7/2}, 2p_{3/2})$ above the $N = 82$ shell gap are included to study neutron-core excitations. The higher core-excited states in ^{132,133}Te are calculated for the first time in this region. The present work well describes both the low-lying and the high-energy states for ^{134}Te, ^{133}Te, and ^{132}Te, as well as the low-lying levels of ^{131}Te and ^{130}Te. The several multiplets with clear boundary exist in ^{134,133}Te, while a new configuration lying between 4.8 and 6.0 MeV is found as a theoretical prediction in ^{134}Te. Finally, the transition probabilities in these nuclei are calculated and compared with available data. The predicted energy levels and electromagnetic transition will be useful for planning future experiments.

DOI: 10.1103/PhysRevC.102.054316

I. INTRODUCTION

The analysis of neutron-rich isotopes in the vicinity of the doubly magic ^{132}Sn is of high interest for both nuclear physics and nuclear astrophysics. The latest experiment, using the recently implemented phase-imaging ion-cyclotron-resonance method, has shown that the $h_{11/2}$ neutron orbital near ^{132}Sn is key for the evolution of the $N = 82$ shell gap towards $Z = 40$ [1]. By the direct observation of single-particle states in odd-mass isotopes close to ^{132}Sn, the doubly magic nature of ^{132}Sn has been reconfirmed in Refs. [2,3]. In 2019, the doubly magic nucleus ^{132}Sn was reconfirmed again by the first charge-radius measurement of a neutron-rich Sn isotope beyond $N = 82$ [4]. For the neutron-rich nuclei near ^{132}Sn, the extended pairing plus multipole-multipole force (EPQQM) model [5–8] provides a good method to describe wholly the low-lying states and cross-shell excitations [9–12]. Recently, this interaction model has been applied to the ($Z > 50$, $N \leqslant 82$) nuclear region "northwest" of ^{132}Sn. The highly excited states above 4.0 MeV are clearly explained in antimony isotopes as excitations across the neutron $N = 82$ shell gap, and the monopole effects of these nuclei also have been examined carefully [13].

As the particle-hole nuclei in the region northwest of ^{132}Sn, the tellurium isotopes have attracted much attention in both experiment and theory [14–20]. The g factor of the 4^+ state in ^{134}Te was measured for the first time through a new technique developed for measuring angular correlations with Gammasphere [14]. Direct insight into the single particle structure is carried by the g factors in nuclei close to doubly closed shells. The yrast states of ^{134}Te above 5.5 MeV are described in terms of valence proton and particle-hole core excitations [21]. The $B(E2)$ of the first excited 2^+ state had been measured in the semimagic nuclide ^{134}Te [22]. Using a ^{248}Cm fission source, the γ rays of ^{132}Sb and ^{133}Te in $N = 81$ isotones have been studied at Gammasphere [23]. The half-life of the $19/2^-$ state in ^{133}Te has been determined on the basis of the new level schemes [24], and the microsecond isomers in ^{130,132}Te have been investigated by thermal neutron induced fission of ^{239}Pu and ^{241}Pu. The 2_2^+ state was identified in ^{132}Te as the one-phonon mixed-symmetry state in a projectile Coulomb excitation experiment that provided a firm example of a mixed-symmetry state in neutron-rich nuclei [25].

In theory, the low-lying level spectrum of ^{134}Te without core excitations has been investigated using shell-model calculations [26,27]. The high-spin states in ^{132}Te have been extended up to an excitation energy of 6.17 MeV, the experimental level scheme has been compared by using the jj55pna interaction without considering neutron-core excitations, and a large energy difference is found in the 17^+ level between the calculation and the experiment [28]. Such experimental findings provide further motivations for performing large-scale shell-model calculations. It is necessary to consider the cross-shell orbits in the natural valence space and to investigate the neutron-core excitations in these neutron-rich nuclei. For example, the $J^\pi = 19/2^+$ state at 1942 keV in ^{133}Ba is identified as an isomer with a half-life of 66.6(20) ns corresponding to a $B(E1)$ value of $7.7 \times 10^{-6}(4)$ e^2fm^2 for the $J^\pi = 19/2^+$ to $J^\pi = 19/2^-$ transition [29]. Due to the cross-shell orbit

*Corresponding author: whk2007@163.com
†Corresponding author: zhli@pku.edu.cn

 ©2020 American Physical Society

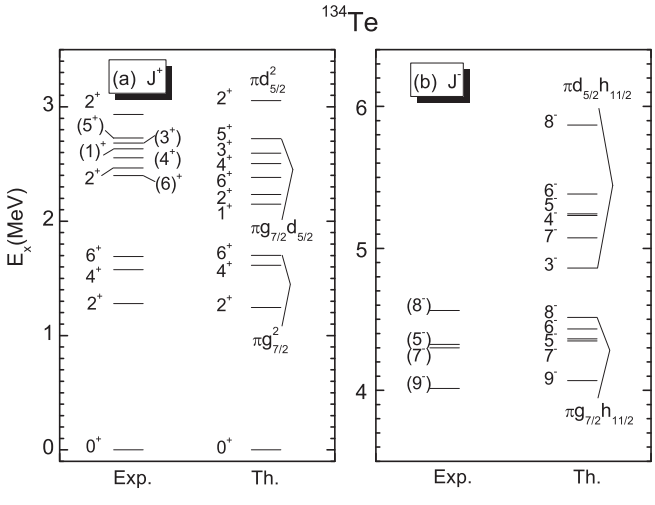

FIG. 1. The theoretical states compared with the known experimental data of ^{134}Te [21,30]: (a) positive-parity states, (b) negative-parity states.

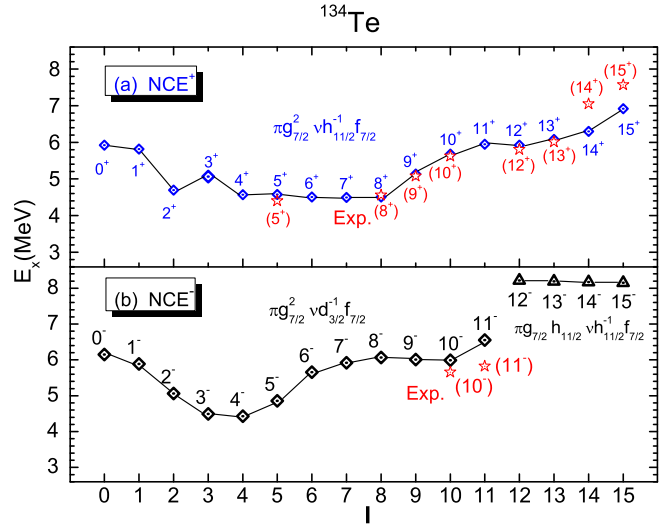

FIG. 2. The theoretical NCE states as a function of spin for ^{134}Te: (a) positive-parity states, (b) negative-parity states. The known experimental data [30] are denoted by asterisks.

$\nu 1f_{7/2}$ included in the model space, the *gdsh* valence space is enlarged to deal with this $E1$ transition.

In this paper, we first briefly mention the Hamiltonian and model space for the sake of completeness. Then we discuss the low-lying and high-energy states in Te isotopes. The higher core-excited states are studied in ^{132,133}Te for the first time. Finally, we discuss the electromagnetic transition in these nuclei for further inspection.

II. RESULTS AND DISCUSSION

In the present work the EPQQM model is applied to study $^{130-134}$Te isotopes by large-scale shell-model calculations. We use the same model space and interaction as in our previous investigation on $^{131-133}$Sb isotopes [13]. The shell-model calculations are carried out in the model space spanned by five proton (neutron) orbits ($0g_{7/2}$, $1d_{5/2}$, $1d_{3/2}$, $2s_{1/2}$, $0h_{11/2}$) between the magic numbers 50 and 82 for proton particles (neutron holes), and no truncation is used in the major shell. Two extra neutron orbits $1f_{7/2}$ and $2p_{3/2}$ above the $N = 82$ shell closure are included for analyzing neutron-core excitations (NCEs). In $^{131-134}$Te, one neutron is allowed to occupy the extra orbit $1f_{7/2}$. For ^{130}Te, the present computational resource is not enough to take NCE into consideration. The experimental data are mainly taken from Refs. [19–21,28,30], and the shell-model code NUSHELLX@MSU is used for calculations [31].

A. ^{134}Te

^{134}Te contains two valence protons outside the ^{132}Sn core. Therefore, the semimagic ^{134}Te nucleus becomes the benchmark to test the proton-proton part of the two-body interaction. Hence a series of experiments have been performed to study the structure of this isotope [21,32–35]. The present calculations reproduce the feature of spherical even-even nuclei that there is large gap (about 1.2 MeV) between ground state 0^+ and first excited state 2^+ [as shown in Fig. 1(a)]. The first 4^+ and 6^+ levels, belonging to the yrast sequence of $\pi g_{7/2}^2$, are also reproduced well.

The other positive-parity states with energy between 2 and 3 MeV are from proton excitation within the major shell. These states have the main configuration of $\pi g_{7/2}d_{5/2}$. The second 4^+ level at 2.504 MeV, with 90% of $\pi g_{7/2}d_{5/2}$, is well reproduced and close to the experimental value at 2.555 MeV. The 6^+ level at 2.384 MeV, which has mostly a pure configuration of $\pi g_{7/2}d_{5/2}$, matches quite well with experimental value 2.398 MeV. The third 2^+ level at 3.055 MeV, which is close to the experimental 2^+ level at 2.934 MeV, has a mixed configuration of 55% of $\pi d_{5/2}^2$, 16% of $\pi g_{7/2}d_{3/2}$, and 14% of $\pi g_{7/2}d_{5/2}$. The 1^+, 3^+, and 5^+ levels also belong to the same sequence. Except for the 1^+ level, the present work well reproduces all the other members of configuration $\pi g_{7/2}d_{5/2}$. The first 1^+ level at 2.15 MeV is a little far from datum 2.632 MeV, while the second 1^+ level lies at 5.016 MeV with a main configuration of $\pi d_{5/2}d_{3/2}$.

The negative-parity states are observed above 4 MeV. These states belong to two multiplets, $\pi g_{7/2}h_{11/2}$ and $\pi d_{5/2}h_{11/2}$. The calculated levels in comparison with experimental data are depicted in Fig. 1(b). The levels of 9^-, 7^-, 5^-, and 8^- from the $\pi g_{7/2}h_{11/2}$ multiplet have good accordance with experimental data in both energy and order. As for the higher excitation energy, a new multiplet with main configuration of $\pi d_{5/2}h_{11/2}$ is predicted, lying from 4.8 to 6 MeV, where the corresponding experimental data are still unavailable.

The higher spin part of the yrast sequence (8^+) to (15^+) was established by Zhang *et al.* [21] and the explanation involves excitations across the ^{132}Sn core. In Fig. 2(a) the states from (8^+) to (13^+) are well reproduced in our calculations, while no datum is available for 11^+ state. We obtain the 11^+ state at 5.999 MeV, close to the value 5.782 MeV in Ref. [21] from the empirical shell-model calculation. The core-excited $\pi g_{7/2}^n \nu h_{11/2}^{-1} f_{7/2}$ levels were obtained in $N = 82$ isotones [21,35]. From our EPQQM calculations, sixteen

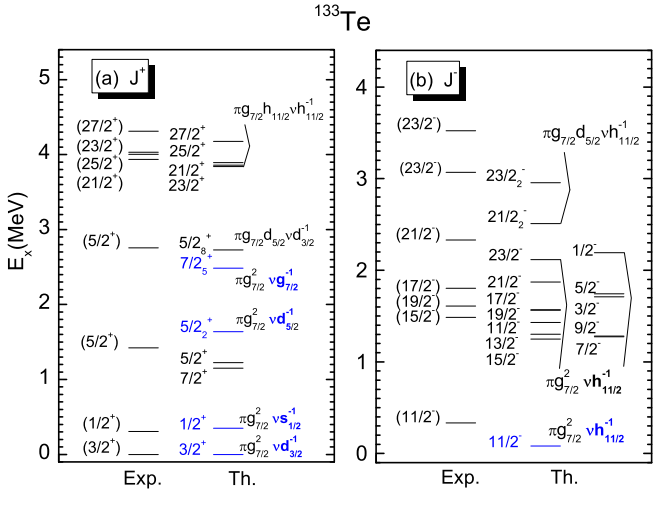

FIG. 3. The theoretical states compared with the known experimental data of ^{133}Te [30].

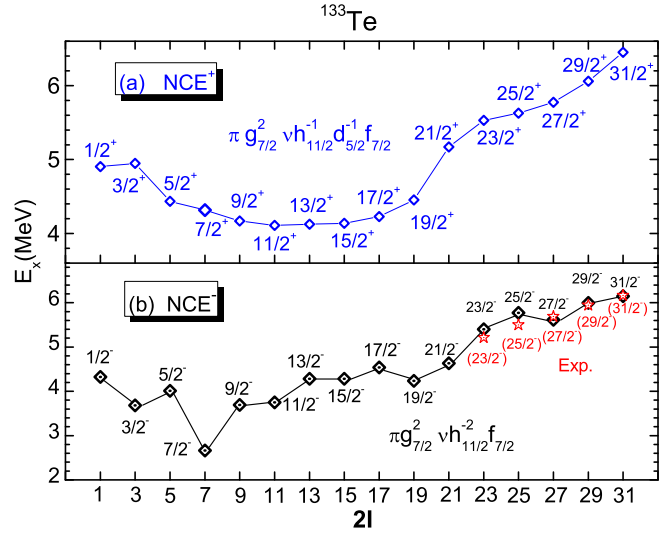

FIG. 4. The theoretical NCE states as a function of spin for ^{133}Te: (a) positive-parity states, (b) negative-parity states. The known experimental data [30] are denoted by asterisks.

members from 0^+ to 15^+ of this sequence are obtained, as shown in Fig. 2(a). The lower spin part of the sequence is not well investigated by experiment, as the yrast (8^+) preferentially decays to the yrast (6^+), leaving it difficult to populate the states with spin $I^\pi < 8^+$. The 5^+ level is known from experiment [36] and we obtained 4.577 MeV by calculation. The two lowest spin states 0^+ and 1^+, with energy around 6 MeV, have more than 90% configuration of $\pi g^2_{7/2}\nu h^{-1}_{11/2} f_{7/2}$. The 2^+ level (at 4.69 MeV) has lower energy compared to 0^+ and 1^+ states, due to about 30% mixture of non-NCE partitions.

The high-spin states 14^+ and 15^+ are 6.297 and 6.919 MeV with main configuration of $\pi g^2_{7/2}\nu h^{-1}_{11/2} f_{7/2}$. Apart from the members of $\pi g^2_{7/2}\nu h^{-1}_{11/2} f_{7/2}$, the $\pi g_{7/2} d_{5/2}\nu h^{-1}_{11/2} f_{7/2}$ has 14^+ and 15^+ levels at 7.12 and 7.72 MeV, which keep accordance with experimental values. In Fig. 2(b), the levels with $I^\pi = 0^-$ to 11^- are shown and these 12 states have a main configuration of $\pi g^2_{7/2}\nu d^{-1}_{3/2} f_{7/2}$. As yrast state, the 10^- level lies close to the datum 5.658 MeV, whereas the 11^- level with 6.552 MeV in theory is a little far from the experimental value 5.822 MeV. Four other nearly degenerate negative-parity states (12^- to 15^-) are also shown in Fig. 2(b). The main configuration of these levels is $\pi g_{7/2} h_{11/2}\nu h^{-1}_{11/2} f_{7/2}$.

B. ^{133}Te

The $N = 81$ isotope ^{133}Te has two protons above the $Z = 50$ shell and one neutron hole below the $N = 82$ shell closure. Therefore, the low-lying excited states of ^{133}Te would arise from coupling of two protons in the $\pi g_{7/2}$ orbital and one neutron hole in $\nu h_{11/2}$. The $11/2^-$ isomer with $t_{1/2} = 55.4$ min at 334 keV was observed in an early measurement [37]. Later, the $\pi g^2_{7/2}\nu h^{-1}_{11/2}$ configuration was extended up to $23/2^-$ [23]. During the same time, the yrast and near yrast particle-hole states were reported up to 6.2 MeV in ^{133}Te using spontaneous fission of ^{252}Cf [24]. As shown in Fig. 3, the ^{133}Te has the same ground state $(3/2^+)$ as in ^{131}Sn, with a main configuration of $\pi g^2_{7/2}\nu d^{-1}_{3/2}$. As the first excited state with positive parity, the $1/2^+$ level has the dominant configuration of $\pi g^2_{7/2}\nu s^{-1}_{1/2}$.

The first $5/2^+$ level is also a member of the sequence $\pi g^2_{7/2}\nu d^{-1}_{3/2}$. On the other hand, the second $5/2^+$ level has two main configurations, about 42% of $\pi g^2_{7/2}\nu d^{-1}_{3/2}$ and about 34% of $\pi g^2_{7/2}\nu s^{-1}_{1/2}$. The $5/2^+$ state at 2.728 MeV matches well with the 2.756 MeV from experiment. We also predict the $7/2^+$ level at energy 2.5 MeV with dominant configuration of $\pi g^2_{7/2}\nu g^{-1}_{7/2}$. The positive states near 4 MeV ($21/2^+$, $25/2^+$, $23/2^+$, $27/2^+$) are well reproduced in the present calculations. This is owing to the fact that the model space used in the calculations is reasonably large and includes the important proton single-particle level $\pi h_{11/2}$. These states near 4 MeV have a main configuration of $\pi g_{7/2} h_{11/2}\nu h^{-1}_{11/2}$, the same as suggested in Ref. [24].

There is a large discrepancy between the first theoretical $23/2^-$ state and the datum of 3.070 MeV $(23/2^-)$, while the second $23/2^-$ state is close to this datum. The value using the jj55pna interaction is 2.5 MeV for this $23/2^-$ level, still some distance from the datum 3.070 MeV. Whether a lower $23/2^-$ state can be observed in further experiment remains unclear.

The negative-parity states and corresponding experimental levels are shown in Fig. 3(b). The first excited negative-parity $11/2^-$ level is obtained at 0.082 MeV with a dominant configuration of $\pi g^2_{7/2}\nu h^{-1}_{11/2}$ (79%). The other members of the sequence, $15/2^-_1$, $17/2^-_1$, $19/2^-_1$, $23/2^-_1$, are from $\pi g^2_{7/2}$ coupled with $\nu h^{-1}_{11/2}$. The $21/2^-_1$ and $23/2^-_2$ levels have the main configuration of $\pi g_{7/2} d_{5/2}\nu h^{-1}_{11/2}$ as suggested in Ref. [24].

As the positive-parity NCE in ^{133}Te, the main configuration of $\pi g^2_{7/2}\nu h^{-1}_{11/2} d^{-1}_{5/2} f_{7/2}$ includes 16 members, from $1/2^+$ to $31/2^+$ levels [Fig. 4(a)]. The negative-parity NCE [Fig. 4(b)] has a main configuration of $\pi g^2_{7/2}\nu h^{-2}_{11/2} f_{7/2}$, which also showed 16 members from $1/2^-$ to $31/2^-$. The data of the high-spin part from $(23/2^-)$ to $(31/2^-)$ are available in

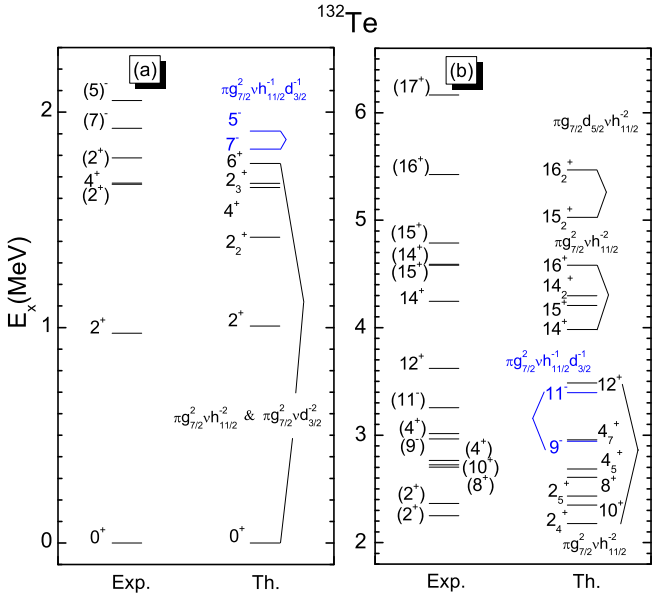

FIG. 5. The theoretical states compared with the known experimental data of ^{132}Te [30]: (a) (0, 2.1 MeV), (b) (2.1, 6.5 MeV).

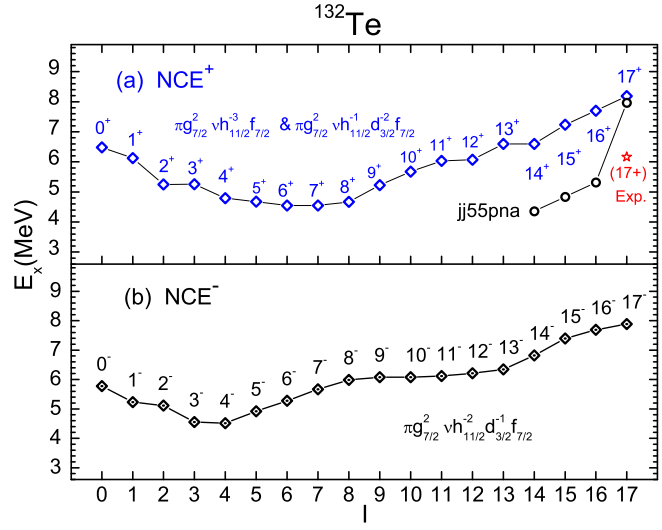

FIG. 6. The calculated NCE states as a function of spin for ^{132}Te: (a) positive-parity states, (b) negative-parity states. The results using the jj55pna interaction are denoted by circles. The known experimental datum (17^+) is denoted by an asterisk.

Ref. [24], and these states are quite well reproduced in the present work. The $7/2^-$ level at 2.665 MeV has the lowest energy, and has a mixed configuration of $\pi g_{7/2}^2 \nu h_{11/2}^{-2} f_{7/2}$ (42%) and $\pi g_{7/2}^2 \nu d_{3/2}^{-2} f_{7/2}$ (18%).

C. ^{132}Te

The structure of low-lying levels in ^{132}Te is dominated by configurations of two proton particles coupled with two neutron holes, which is more complex compared to ^{133,134}Te. For example, the ground state 0^+ has about five different configurations. The two major ones are shown in Fig. 5. In those five configurations, the proton part is the same as $\pi g_{7/2}^2$, whereas the neutron parts are $\nu d_{3/2}^{-2}$, $\nu h_{11/2}^{-2}$, $\nu s_{1/2}^{-2}$, $\nu d_{5/2}^{-2}$, and $\nu g_{7/2}^{-2}$ respectively. The $\pi g_{7/2}^2 \nu h_{11/2}^{-2}$ and $\pi g_{7/2}^2 \nu d_{3/2}^{-2}$ are also the dominant configurations for 2_1^+ to 6_1^+ levels [Fig. 5(a)], as well as 2_5^+ [Fig. 5(b)].

With the main configuration of $\pi g_{7/2}^2 \nu h_{11/2}^{-2}$, the four levels of 10^+, 8^+, 4_5^+, and 4_7^+ match the known experimental data well (Fig. 5). As a member of proton $\pi g_{7/2} d_{5/2}$, the 2_4^+ level has a different configuration compared to other nearby states. The five levels from 12^+ to 16^+ with energy below 5 MeV belong to the $\pi g_{7/2}^2 \nu h_{11/2}^{-2}$ sequence. The 12^+ level at 3.711 MeV is close to the datum 3.622 MeV. The energy and ordering of 14_1^+, 15_1^+, and 14_2^+ states are well reproduced in our calculations. Note that the level (16^+) at 4.836 MeV is a little far from the experimental level at 5.424 MeV. The two levels at the top in Fig. 5(b), 15_2^+ and 16_2^+, have very pure configuration of $\pi g_{7/2} d_{5/2} \nu h_{11/2}^{-2}$ (more than 90%).

Compared to the experimental (17^+) level at 6.17 MeV, the 17^+ level using jj55pna has a large energy difference. The 17^+ level of NCE in the present work is also a little far from this (17^+) level in experiment, while the 17^+ level in the natural valence space lies at 8.778 MeV with main configuration of $\pi g_{7/2} h_{11/2} \nu g_{7/2}^{-1} h_{11/2}^{-1}$. Due to the Pauli principle, the level 17^+ could not be produced by the sequence $\pi g_{7/2}^2 \nu h_{11/2}^{-2}$.

The negative-parity states are shown in Fig. 5 in comparison with known data. The 7^- level at 1.829 MeV has about 70% of $\pi g_{7/2}^2 \nu h_{11/2}^{-1} d_{3/2}^{-1}$, that is well accordance with the experimental value 1.925 MeV. The 5^+ level at 1.911 MeV has two main configurations, about 43% of $\pi g_{7/2}^2 \nu h_{11/2}^{-1} d_{3/2}^{-1}$ and about 28% of $\pi g_{7/2}^2 \nu h_{11/2}^{-1} s_{1/2}^{-1}$. The 9_1^- level at 2.951 MeV has dominant configuration $\pi g_{7/2}^2 \nu h_{11/2}^{-1} d_{3/2}^{-1}$, and the 11^- level at 3.394 MeV belongs to the sequence of $\pi g_{7/2}^2 \nu h_{11/2}^{-1} d_{3/2}^{-1}$.

The core excited states in ^{132}Te have a little higher energy in comparison with ^{134}Te. The positive parity of neutron-core excited levels with $I^\pi = 0^+$ to 17^+ have two main configurations, $\pi g_{7/2}^2 \nu h_{11/2}^{-3} f_{7/2}$ and $\pi g_{7/2}^2 \nu h_{11/2}^{-1} d_{3/2}^{-2} f_{7/2}$. The partition $\pi g_{7/2}^2 \nu h_{11/2}^{-3} f_{7/2}$ contributes largely for the lowest $(0^+, 1^+, 2^+)$ and the highest spins (16^+ and 17^+). The negative parity of NCE in Fig. 6(b) also has two main configurations, about 50% of $\pi g_{7/2}^2 \nu h_{11/2}^{-2} d_{3/2}^{-1} f_{7/2}$ and about 10% of $\pi g_{7/2}^2 \nu h_{11/2}^{-1} s_{1/2}^{-1} f_{7/2}$ in average. The 4^- level at 4.518 MeV has a main configuration of $\pi g_{7/2}^2 \nu h_{11/2}^{-2} d_{3/2}^{-1} f_{7/2}$ (about 53%). So far no cross-shell excitation has been observed in ^{132}Te.

D. ^{131,130}Te

With three neutron holes below $N = 82$, the nucleus ^{131}Te still has the ground state $(3/2^+)$ as in ^{131}Sn. The main configuration is about 59% of $\pi g_{7/2}^2 \nu h_{11/2}^{-2} d_{3/2}^{-1}$ (Fig. 7). As the first excited positive parity, the $1/2^+$ level has the main configuration of $\pi g_{7/2}^2 \nu h_{11/2}^{-2} s_{1/2}^{-1}$. As shown in Fig. 7, the dominant configuration of the yrast sequence is $\pi g_{7/2}^2 \nu h_{11/2}^{-2} d_{3/2}^{-1}$ for $I^\pi = 3/2^+$ to $17/2^+$. As for $21/2^+$ state, the two configurations have nearly equal contributions. For the highest spin states, $23/2^+$ and $25/2^+$, the configuration $\pi g_{7/2}^2 \nu h_{11/2}^{-2} s_{1/2}^{-1}$

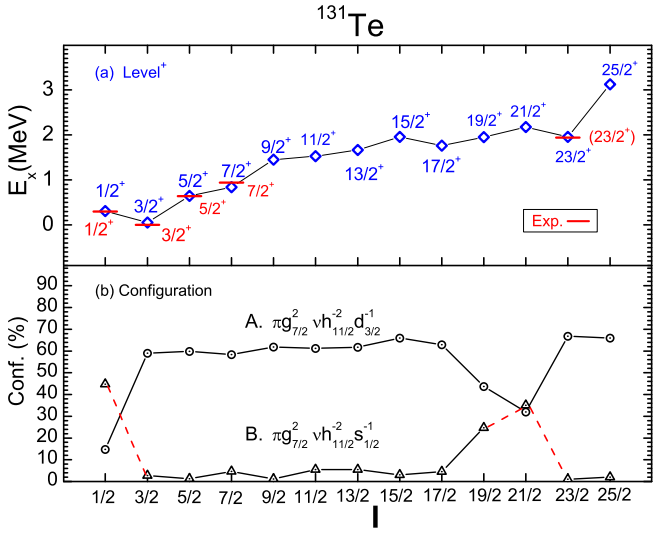

FIG. 7. The calculated positive-parity states (a) and the percentage of main configurations as a function of spin for ^{131}Te (b). The known experimental data [30] are denoted by the red solid line.

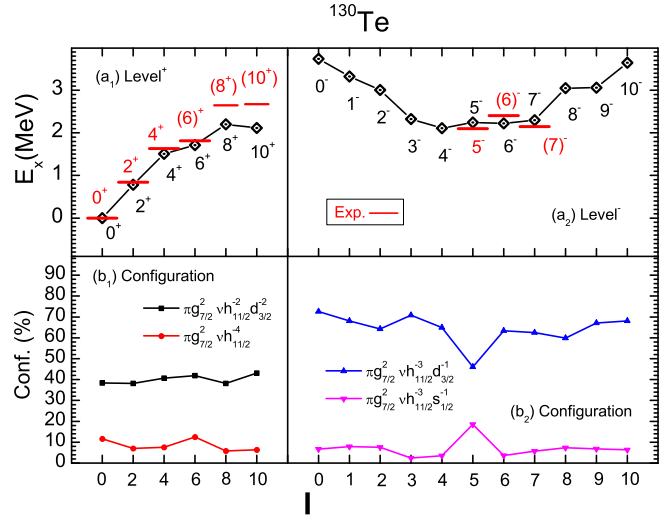

FIG. 9. The theoretical low-lying levels (a_1, a_2) and the percentage of main configurations (b_1, b_2) as a function of spin for ^{130}Te. The known experimental data [30] are denoted by the red solid line.

becomes dominant. As shown in Fig. 8, the negative-parity levels have more complex configurations, where the largest contribution (about 30%) comes from $\pi g^2_{7/2}\nu h^{-1}_{11/2}d^{-2}_{3/2}$ except for $9/2^-$ and $25/2^-$ levels. The $9/2^-$ level has about 40% contribution from $\pi g^2_{7/2}\nu h^{-3}_{11/2}$ and the $25/2^-$ level has about 29% contribution from $\pi g^2_{7/2}\nu h^{-1}_{11/2}s^{-1}_{1/2}d^{-1}_{3/2}$. Besides the five experimental states from $3/2^-$ to $11/2^-$, the high spin $(19/2^-)$ level is very close to the experimental data.

For ^{130}Te, the cross-shell orbits are frozen due to the limitation of computational power, while only the low-lying levels are shown in Fig. 9. The dominant configuration is $\pi g^2_{7/2}\nu h^{-2}_{11/2}d^{-2}_{3/2}$ ($\pi g^2_{7/2}\nu h^{-3}_{11/2}d^{-1}_{3/2}$) for positive (negative) parity levels. For the negative-parity sequence, the configuration $\pi g^2_{7/2}\nu h^{-3}_{11/2}s^{-1}_{1/2}$ has an average share of about 10%, except the 5^- level is up to about 20%. The dominant configuration has an obvious declination in this 5^- level correspondingly.

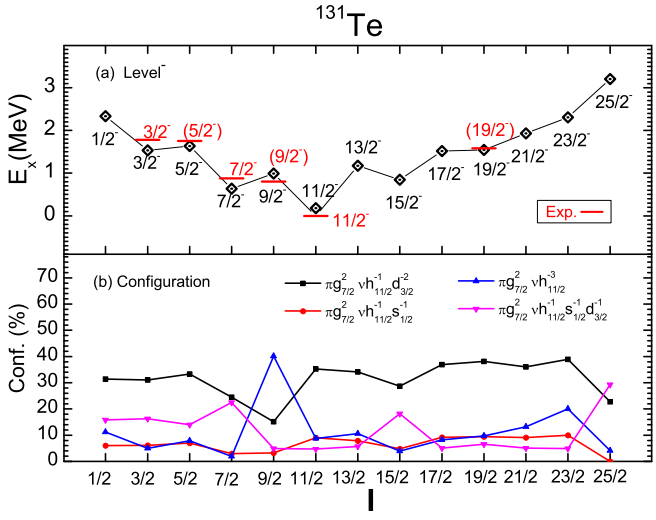

FIG. 8. The calculated negative-parity states (a) and the percentage of main configurations as a function of spin for ^{131}Te (b). The known experimental data [20,30] are denoted by the red solid line.

E. Electromagnetic transition

The electromagnetic transition serves as the strict test for the wave functions obtained from shell-model calculations. The calculated results are compared with available experimental data for $E\lambda$ and $M\lambda$ transition in Te isotopes in Table I. The standard effective charge of $e_\pi = 1.5e$ ($e_\nu = 0.5e$) is used for the proton (neutron) during the present calculations. With quenching factor 0.70, the g factors $g^\pi_l = 1$, $g^\nu_l = 0$, $g^\pi_s = 3.910$, and $g^\nu_s = -2.678$ are used for magnetic transition. Noting that the g factor is sensitive to the two-body interactions, we test the g factors in ^{134}Te by comparing with data in Ref. [14]. The g factor 0.68 of the 4^+ level in this work is within the experimental data $\pm 0.70^{+0.55}_{-0.38}$. It is also close to previous calculations, 0.72 [14] and 0.83 [15].

For the $E2$ transitions, overall agreement is obtained in the nuclei $^{131-134}$Te with NCE. The average difference is the factor 1.24, while the largest difference is the factor 1.55 in ^{131}Te from $17/2^-$ to $13/2^-$. However, the $E2$ transitions in ^{130}Te are not satisfactorily reproduced. For example the difference is the factor 2.0 (2.4) for $2^+ \to 0^+$ ($6^+ \to 4^+$). This could be mainly due to the frozen cross-shell orbits. For example, the $E2$ values will decrease on average to about 80% in ^{134}Te and about 70% in ^{132}Te without NCE. Assuming the $E2$ value 7.467 W.u. in ^{130}Te from 2^+ to 0^+ is only 75% of the one within NCE, the difference will be the factor 1.52 with the datum 14.9(5) W.u., which is close to the performance in $^{131-134}$Te.

The $E1$ transition from 7^- to 6^+ in ^{132}Te provides acceptable performance in the present work. The cross-shell orbit

TABLE I. The theoretical electromagnetic transition probabilities in ^{134,133,132}Te and compared with the known experimental data [19,20,22,25,30].

Transition	τL	Expt. (W.u.)	Theor. (W.u.)
^{134}Te			
$2^+ \to 0^+$	$E2$	5.1 (2)	4.773
$4^+ \to 2^+$	$E2$	4.3 (4)	4.989
$6^+ \to 4^+$	$E2$	2.05 (4)	2.342
$(6^+) \to 6^+$	$E2$		0.541
$(9^-) \to (6^+)$	$E3$	8.2 (3)	7.512
$(9^-) \to 6^+$	$E3$	3.80 (14)	1.071
^{133}Te			
$(11/2^-) \to (3/2^+)$	$M4$	4.7 (6)	9.81
$(19/2^-) \to (15/2^-)$	$E2$	2.56 (14)	2.829
^{132}Te			
$2^+ \to 0^+$	$E2$	10 (1)	7.414
$2_2^+ \to 2_1^+$	$M1$	3.02 (1.96) & (>0.128)	0.070
$4^+ \to 2^+$	$E2$		6.588
$6^+ \to 4^+$	$E2$	3.3 (2)	3.722
$(8^+) \to 6^+$	$E2$		0.00306
$(10^+) \to (8^+)$	$E2$	1.05 (3)	0.745
$(7^-) \to 6^+$	$E1$	2.56×10^{-9} (14)	5.399×10^{-9}
$(5^-) \to 4^+$	$E1$		2.898×10^{-6}
$(10^+) \to (7^-)$	$E3$		5.674×10^{-3}
^{131}Te			
$(23/2)^+ \to (17/2)^-$	$E3$		2.645×10^{-5}
$(23/2)^+ \to (19/2^-)$	$M2$	1.9×10^{-6}	1.612×10^{-4}
$(17/2)^- \to (13/2)^-$	$E2$	3.5 (10)	2.255
$(13/2)^- \to (11/2)^-$	$E2$		8.125
$(11/2)^- \to (3/2)^+$	$M4$	4.59 (12)	0.00338
^{130}Te			
$2^+ \to 0^+$	$E2$	14.9 (5)	7.467
$4^+ \to 2^+$	$E2$		10.266
$6^+ \to 4^+$	$E2$	6.1 (3)	2.502

$1f_{7/2}$ is necessary for reproducing the $E1$ transition. Without cross-shell orbits in the present model space, the $E1$ value will be zero. For the $E1$ transition from 7^- to 6^+ in ^{132}Te, only about 1% of configurations in the two states contribute to the tiny $E1$ transition, and a datum close to zero was observed in experiment. This is direct evidence of neutron-core excitations in this nuclei region. For the states involved in the $E1$ transition listed in Table I, their wave functions have about 1% percent of configurations including $(1d_{5/2}, 1f_{7/2})$ or $(0g_{7/2}, 1f_{7/2})$, which may be coupled to the low-lying 1^- spuriosities. With an effect of order $1/A$ (A, mass), such a spurious center-of-mass problem can be neglected for the heavy nuclei [38].

For the other transitions, the $B(E3)$ from (9^-) to 6^+ is smaller in comparison with experimental value 3.80 (14) W.u. In ^{133}Te, the theoretical value (9.81 W.u.) of the $M4$ transition from $(11/2^-)$ to $(3/2^+)$ has a difference of factor 2.1, comparing to datum 4.7 (6) W.u. In ^{132}Te, a large $M1$ value in experiment was obtained from (2_2^+) to 2_1^+, and the shell-model calculations reproduce the lower limit [25]. Also a smaller value is obtained for this $M1$ in the present work. In ^{131}Te, the transition rates from $(23/2^-)$ state to the ground state $3/2^+$ via intermediate levels are calculated and compared with experimental data. The datum 1580 keV was suggested as $(17/2)^-$ with $B(E3) = 0.0151(20)$ from $(23/2^+)$ [30], while the theoretical $E3$ value is 2.645×10^{-5} W.u. In Ref. [20], a $(19/2^-)$ state is measured around the energy 1580 keV, and the $M2$ multipolarity from $(23/2)^+$ to this level leads to $B(M2) = 1.9 \times 10^{-6}$ W.u. The present work gets the value of 3.172×10^{-4} W.u. for this $B(M2)$. On the whole, our shell-model calculations with NCE provide satisfactory descriptions of the electromagnetic transition in Te isotopes.

III. CONCLUSION

We have performed large-scale shell-model calculations with the extended pairing plus multipole-multipole force and neutron-core excitations for the neutron-rich particle-hole nuclei in $^{131-134}$Te close to ^{132}Sn. The main conclusions for the present study are summarized as follows:

(1) The low-lying and high-energy states in ^{133,134}Te can be well described by coupling valence nucleons and neutron-core excitations. The available experimental data are reproduced well.
(2) Several multiplets with clear boundary are found in ^{133,134}Te for both experiment and theory, and the low-lying multiplets of the ^{133}Te nucleus lie close to those of ^{134}Te.
(3) The higher core-excited states in ^{132,133}Te are theoretically investigated for the first time in this work. Except for the lowest $7/2^+$ level at about 2.7 MeV, all core-excited states lie above 4.0 MeV in ^{133}Te, which is good evidence for the robustness of the $N = 82$ shell closure. Experimental information about core-excited states in ^{132,133}Te are still rather limited. The predicted results can provide guidance for the planning of future experiments.
(4) In ^{132}Te, the experimental data lying between 4 and 6 MeV correspond to configurations of $\pi g_{7/2}^2 \nu h_{11/2}^{-2}$ and $\pi g_{7/2} d_{5/2} \nu h_{11/2}^{-2}$ in the natural valence space. The neutron-core excitation states are produced from 6.5 to 8.0 MeV with spin-parity $I^\pi = 14^+$ to 16^+.
(5) The transition probabilities of $E1$, $E2$, $E3$, $M2$, and $M4$ are calculated and compared with known experimental data. The $E1$ transition in ^{132}Te from 7^- to 6^+ was reproduced very well in the present work, which provides direct evidence of neutron-core excitation in this nuclei region.
(6) Due to the present descriptions of both energy levels and electromagnetic transition, the present Hamiltonian provides overall agreement in the particle-hole nuclei near doubly-magic ^{132}Sn. The predictions will be profitable for the prospective experiments in this neutron-rich nuclei region.

ACKNOWLEDGMENTS

We thank Hua Jin and Cen Xi Yuan for useful discussions. Research at GSI is supported by the China and Germany

Postdoctoral Exchange Fellowship Program 2019 from the Office of China Postdoctoral Council (No. 20191024). Research at Zhoukou Normal University is supported by the National Natural Science Foundation of China (No. 11505302). Research at SJTU is supported by the National Natural Science Foundation of China (No. 11575112, No. 11135005, No. 11505302) and by the 973 Programs of China (No. 2013CB834401, No. 2016YFA0400501). Research at Peking University is supported by the National Natural Science Foundation of China (No. 11775003).

[1] V. Manea, J. Karthein, D. Atanasov, M. Bender, K. Blaum, T. E. Cocolios, S. Eliseev, A. Herlert, J. D. Holt, W. J. Huang *et al.*, Phys. Rev. Lett. **124**, 092502 (2020).
[2] K. L. Jones *et al.*, Nature (London) **465**, 454 (2010).
[3] K. L. Jones *et al.*, Phys. Rev. C **84**, 034601 (2011).
[4] C. Gorges, L. V. Rodrífuez, D. L. Balabanski, M. L. Bissell, K. Blaum, B. Cheal, R. F. Garcia Ruiz, G. Georgiev, W. Gins, H. Heylen *et al.*, Phys. Rev. Lett. **122**, 192502 (2019).
[5] M. Hasegawa, K. Kaneko, and S. Tazaki, Nucl. Phys. A **688**, 765 (2001).
[6] K. Kaneko, M. Hasegawa, and T. Mizusaki, Phys. Rev. C **66**, 051306(R) (2002).
[7] K. Kaneko, Y. Sun, M. Hasegawa, and T. Mizusaki, Phys. Rev. C **78**, 064312 (2008).
[8] K. Kaneko, Y. Sun, T. Mizusaki, and M. Hasegawa, Phys. Rev. C **83**, 014320 (2011).
[9] H. K. Wang, Y. Sun, H. Jin, K. Kaneko, and S. Tazaki, Phys. Rev. C **88**, 054310 (2013).
[10] H. K. Wang, K. Kaneko, and Y. Sun, Phys. Rev. C **89**, 064311 (2014).
[11] H.-K. Wang, K. Kaneko, and Y. Sun, Phys. Rev. C **91**, 021303(R) (2015).
[12] H. K. Wang, K. Kaneko, Y. Sun, Y. Q. He, S. F. Li, and J. Li, Phys. Rev. C **95**, 011304(R) (2017).
[13] H. K. Wang, S. K. Ghorui, K. Kaneko, Y. Sun, and Z. H. Li, Phys. Rev. C **96**, 054313 (2017).
[14] C. Goodin, N. J. Stone, A. V. Ramayya, A. V. Daniel, J. R. Stone *et al.*, Phys. Rev. C **78**, 044331 (2008).
[15] B. A. Brown, N. J. Stone, J. R. Stone, I. S. Towner, and M. Hjorth-Jensen, Phys. Rev. C **71**, 044317 (2005).
[16] D. C. Radford, C. Baktash, J. R. Beene *et al.*, Phys. Rev. Lett. **88**, 222501 (2002).
[17] K. Sieja, G. Martinez-Pinedo, L. Coquard, and N. Pietralla, Phys. Rev. C **80**, 054311 (2009).
[18] S. Sarkar and M. S. Sarkar, Phys. Rev. C **64**, 014312 (2001).
[19] C. J. Barton, M. A. Caprio, D. Shapira, N. V. Zamfir, D. S. Brenner, R. L. Gill, T. A. Lewis, J. R. Cooper, R. F. Casten, C. W. Beausang *et al.*, Phys. Lett. B **551**, 269 (2003).
[20] A. Astier, M.-G. Porquet, Ts. Venkova *et al.*, Eur. Phys. J. A **50**, 2 (2014).
[21] C. T. Zhang, P. Bhattacharyya, P. J. Daly, R. Broda, Z. W. Grabowski, D. Nisius *et al.*, Phys. Rev. Lett. **77**, 3743 (1996).
[22] A. E. Stuchbery, J. M. Allmond, A. Galindo-Uribarri, E. Padilla-Rodal, D. C. Radford, N. J. Stone, J. C. Batchelder, J. R. Beene, N. Benczer-Koller, C. R. Bingham, M. E. Howard, G. J. Kumbartzki, J. F. Liang, B. Manning, D. W. Stracener, and C. H. Yu, Phys. Rev. C **88**, 051304(R) (2013).
[23] P. Bhattacharyya *et al.*, Phys. Rev. C **64**, 054312 (2001).
[24] J. K. Hwang, A. V. Ramayya, J. H. Hamilton, C. J. Beyer *et al.*, Phys. Rev. C **65**, 034319 (2002).
[25] M. Danchev, G. Rainovski, N. Pietralla *et al.*, Phys. Rev. C **84**, 061306(R) (2011).
[26] S. H. Liu *et al.*, Phys. Rev. C **81**, 014316 (2010).
[27] L. Coraggio, A. Covello, A. Gargano, N. Itaco, and T. T. S. Kuo, Phys. Rev. C **80**, 044320 (2009).
[28] S. Biswas *et al.*, Phys. Rev. C **93**, 034324 (2016).
[29] L. Kaya, A. Vogt, P. Reiter *et al.*, Phys. Rev. C **100**, 024323 (2019).
[30] Data extracted using the NNDC On-line Data Service from the ENSDF database, with cutoff dates of July 31, 2004; October 31, 2010; and February 10, 2005 for ^{134}Te, ^{133}Te, and ^{132}Te, respectively.
[31] B. A. Brown and W. D. M. Rae, Nucl. Data Sheets **120**, 115 (2014).
[32] B. Fogelberg, B. Ekström, L. Sihver, and G. Rudstam, Phys. Rev. C **41**, R1890 (1990).
[33] J. P. Omtvedt, H. Mach, B. Fogelberg, D. Jerrestam, M. Hellström, L. Spanier, K. I. Erokhina, and V. I. Isakov, Phys. Rev. Lett. **75**, 3090 (1995).
[34] P. J. Daly, C. T. Zhang, P. Bhattacharyya, R. Broda, Z. W. Grabowski, D. Nisius *et al.*, Z. Phys. A **358**, 203 (1997).
[35] S. K. Saha, C. Constantinescu, P. J. Daly, P. Bhattacharyya, C. T. Zhang, Z. W. Grabowski *et al.*, Phys. Rev. C **65**, 017302 (2001).
[36] A. A. Sonzogni, Nucl. Data Sheets **103**, 1 (2004).
[37] *Table of Isotopes*, 8th ed., edited by R. B. Firestone and V. S. Shirley (Wiley Interscience, New York, 1996), and references therein.
[38] H. Jin, S. Tazaki, K. Kaneko, H.-K. Wang, and Y. Sun, Phys. Rev. C **100**, 064316 (2019).